Available online at www.sciencedirect.com
ScienceDirect
Journal of the European Ceramic Society 27 (2007) 2333–2340
www.elsevier.com/locate/jeurceramsoc

Extrusion and property characterisation of waste-based ceramic formulations

F. Raupp-Pereira [a], M.J. Ribeiro [b], A.M. Segadães [a], J.A. Labrincha [a,*]

[a] *Ceramics and Glass Engineering Department, CICECO, University of Aveiro, 3810-193 Aveiro, Portugal*
[b] *ESTG, Polytechnique Institute of Viana do Castelo, 4900-348 Viana do Castelo, Portugal*

Received 7 May 2006; received in revised form 12 July 2006; accepted 21 July 2006
Available online 12 September 2006

Abstract

This work describes the studies carried out with various industrial wastes and natural sub-products based on the SiO_2–Al_2O_3–CaO system, aimed at extruding all-waste ceramic products of industrial interest. Four waste materials were selected and characterised, namely, (i) Al-rich anodising sludge (A-sludge), (ii) sludge from the filtration/clarification of potable water (W-sludge), (iii) sludge generated in marble sawing processes (M-sludge), and (iv) foundry sand (F-sand).

The plastic behaviour of two different all-waste formulations was first characterised by stress–strain curves and then, after prior adjustment of the plasticity level, the effect of the ram speed and extrusion pressure was evaluated using the Benbow–Bridgwater's model for paste extrusion. Using the waste-based formulations with additives and tube-dies of different die-land dimensions, a good agreement was demonstrated between predicted and measured values. The differences in the static friction coefficient give an effective indication of the surface quality of the extrudate.

Extruded rods were then fired at several temperatures and characterised in terms of relevant functional properties (shrinkage, density and mechanical strength). Compositional evolution was assessed by X-ray diffraction. Since interesting performances were observed, the potential of the use of wastes in ceramic formulations of industrial interest was confirmed.

Keywords: Recycling; Extrusion; Strength

1. Introduction

Traditionally, waste materials are disposed of as soil conditioners or in land filling. However, there might be reusing or recycling alternatives that should be investigated and eventually implemented.[1–10] The extraction of mineral resources from the ground and their transformation are good examples of this scenario.[11] Industrial processes like aluminium anodising and powder surface coating, are highly water consuming and, in the end, a huge flow of wastewater has to be treated, leading to the formation of high amounts of sludge.[9] Even the basic activity of water filtration/clarification for human consumption generates a significant volume of sludge.[12]

In general, the composition of a specific waste product reflects its source, showing various levels of contamination according to the processing/conditioning methods. In terms of chemical composition, the dominant oxide in the great majority of waste materials is silica (SiO_2), closely followed by alumina and lime (Al_2O_3, CaO), and finally by fluxing oxides (alkalies and iron). If a prediction is needed, of the effect and/or the role of the waste material within a given process or product, it can be looked for in the system SiO_2–Al_2O_3–CaO–(Na_2O, K_2O, iron oxide). The system phase diagram can provide valuable estimates of the proportions of phases present during and after firing, namely, the presence of a liquid phase at the firing temperature and the resulting major crystalline phases.[8,9,12]

However, green processing difficulties are frequently the reason that precludes the use of many a raw material. Given that extrusion is commonly used in the manufacture of ceramic products of industrial interest, previous work has been aimed at exploring the applicability of the known Benbow–Bridgwater mathematical model for paste extrusion[13,14] to ceramic formulations containing waste materials.[15,16] Benbow et al.[13,14] showed that the total pressure (P) needed to extrude particulate pastes, comprising fine particles suspended in a liquid continuous phase, through dies with circular cross-section and having a square

* Corresponding author. Tel.: +351 234370250; fax: +351 234425300.
E-mail address: jal@cv.ua.pt (J.A. Labrincha).

0955-2219/$ – see front matter © 2006 Elsevier Ltd. All rights reserved.
doi:10.1016/j.jeurceramsoc.2006.07.015

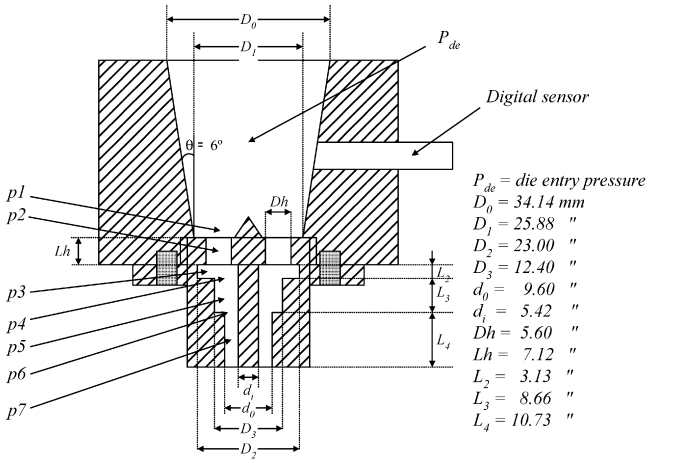

Fig. 1. Detailed representation of the 30*L* die used in ram extrusion of hollow-tubes. The 120*L* die design is similar, but with L_4 = 99.0 mm.

entry, is the sum of the die-entry (P_{de}) and die-land (P_{dl}) pressures and can be described by:

$$P = P_{de} + P_{dl} = 2(\sigma_0 + \alpha V^n) \ln\left(\frac{D_0}{D}\right) + (\tau_0 + \beta V^m) 4\left(\frac{L}{D}\right) \quad (1)$$

In Eq. (1), α is a rate-dependent factor for the convergent flow, β the rate-dependent factor for parallel flow, n and m exponents, σ_0 the paste bulk yield value, τ_0 the paste characteristic initial wall shear stress, D_0 and D the diameters of the barrel and of the die, respectively, L the die-land length and V is the extrudate velocity. A key parameter for controlled extrusion[17] is the coefficient of static friction for the extrudate (μ) which can be calculated by the relationship:

$$\mu = \frac{\tau_0}{\sigma_0} \quad (2)$$

When dies with complex geometry are used, the model equations can be suitably modified,[13,14,18] specially to encompass the various contributions to the die-land pressure (P_{dl}), as shown in Eqs. (3) and (4) and Fig. 1:

$$P_{de} = 2(\sigma_0 + aV^n + \tau_0 \cot\theta) \ln\left(\frac{D_0}{D_1}\right) + \beta V^m \cot\theta \quad (3)$$

$$\begin{aligned} P_{dl} &= p1 + p2 + \cdots + p7 \\ &= \left[2\left(\sigma_0 + \alpha\left(\frac{4Q}{\pi D_h^2 N}\right)^n\right) \ln\left(\frac{D_1}{D_h\sqrt{N}}\right)\right] \\ &\quad + \left[4\left(\tau_0 + \beta\left(\frac{4Q}{\pi D_h^2 N}\right)^m\right)\left(\frac{L_h}{D_h}\right)\right] \\ &\quad + \left[(\tau_0 + \beta V^m)\left(\frac{L_2 M_2}{A_2}\right)\right] + \left[\ln\left(\frac{A_2}{A_3}\right)(\sigma_0 + \alpha V^n)\right] \\ &\quad + \left[(\tau_0 + \beta V^m)\left(\frac{4L_3}{D_3 - d_i}\right)\right] + \left[\ln\left(\frac{A_3}{A_4}\right)(\sigma_0 + \alpha V^n)\right] \\ &\quad + \left[(\tau_0 + \beta V^m)\left(\frac{4L_4}{d_0 - d_i}\right)\right] \end{aligned} \quad (4)$$

In Eqs. (3) and (4), N is the number of internal holes with diameter D_h, Q the volumetric flow rate, A_x the cross-section area at location x, M_x the perimeter length at the location x, L_x the die-land length at location x and θ is the angle of the die-entry region.

In the earlier works, after characterising the plastic behaviour by stress–strain curves,[15] the effect of the ram speed and pressure was evaluated using the Benbow–Bridgwater model. In general, predicted and measured values were found to be in good agreement. Differences in the static friction coefficient (μ), due to different initial wall shear stress (τ_0), gave effective information about the surface quality of the extrudate.[16]

The present work tests the applicability of the Benbow–Bridgwater model in the extrusion of ceramic products of industrial interest (tubes, using dies of different die-land dimensions) and is an extension of those earlier studies, as it describes the studies carried out on all-waste ceramic compositions, based on the SiO_2–Al_2O_3–CaO system, and includes the characterisation of the final fired products in terms of relevant functional properties (shrinkage, density and mechanical strength).

2. Experimental

Four waste materials were selected and characterised, namely: (i) Al-rich anodising sludge (A-sludge), that was firstly calcined at 1400 °C and milled (6.5 μm final average particle size); (ii) sludge from the filtration/clarification of potable water (W-sludge); (iii) sludge generated in marble sawing processes (M-sludge); and (iv) foundry sand (F-sand) that was milled and sieved through 75 μm. W- and M-sludges were used in the as-received condition. Their full characterisation is detailed elsewhere.[8,9,12]

Two different formulations (named A and B) were prepared, combining those materials in the proportions given in Table 1, in the form of aqueous suspensions with a solids load of 30–35 wt.%. These suspensions were deagglomerated and homogenised by wet ball milling during 15 h.

The slurries were then dehydrated in plaster moulds up to water contents of ~20 wt.%, which was found suitable for extrusion. After dehydration and in order to adjust the pastes plasticity, commercial additives were used: 8 wt.% plasticizer (Zusoplast C28) and 2 wt.% lubricant (Zusoplast O59), both from Zschimmer & Schwarz (Germany).

The yield value and plasticity level of each paste were obtained from stress–strain tests carried out by plastic compression (Lloyd Instruments LR 30K, 500 N load cell) in metal moulds. The formulations were pre-extruded through a cylindrical die (33.0 mm in diameter), to improve mixing and homogeneity, and cut into test billets (43.0 mm length). A minimum of three specimens per composition was tested. Compression tests were

Table 1
Tested paste formulations (wt.%)

Mixture	A-calc	W-sludge	M-sludge	F-sand
A	70.0	5.0	20.0	5.0
B	30.0	20.0	25.0	25.0

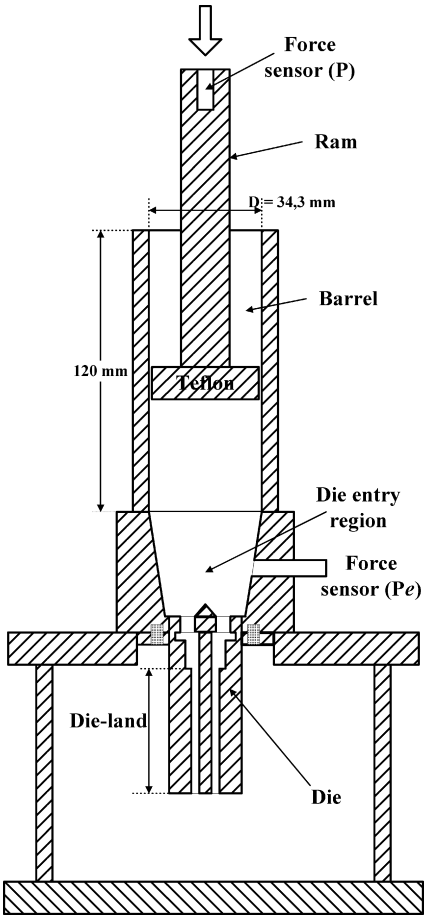

Fig. 2. Ram extruder apparatus used in the extrusion tests.

conducted under a constant cross-head speed of 2.0 mm/min until a maximum deformation of ~70% or the ultimate limit of the load cell was reached.[15]

Extrusion tests were performed in a ram extruder using two dies with 30 and 120 mm die-land lengths (referenced as 30*L* and 120*L*, respectively). Tested ram velocities were: 1, 2, 5, 10, 20, 30, 60, 100 and 200 mm/min. Fig. 2 shows a general view of the apparatus, whose die region and all the contributing pressure drops were detailed in Fig. 1. Values of total pressure (P) applied through the ram and of the die-land pressure (P_{dl}) were measured with digital sensors.

Extruded bodies (20 cm long rods) were dried (overnight at 40 °C + 2 h at 110 °C) and then fired at various temperatures, with heating and cooling rates of 10 °C/min and 1 h soaking at maximum temperature. Samples of composition A were fired at 1350, 1450 and 1550 °C, and those of composition B, at 1350, 1400 and 1450 °C.

The characterisation of dried and fired samples included common ceramic parameters: linear shrinkage, 3-point flexural strength (Lloyd Instruments LR 30K), apparent density (Hg displacement Archimedes method), and water absorption (water displacement Archimedes method, after 2 h in boiling water). The mineralogical characterisation, to identify the major crystalline phases formed during firing, was carried out by XRD (Rigaku Denk Co., Japan). The microstructure evolution was studied by SEM (Hitachi S4100) on fractured and polished samples, after chemical etching (2 v/v, HF solution for 1 min) or thermal etching (~10 min at a temperature 10% lower than the sintering value).

3. Results and discussion

3.1. Plastic and extrusion behaviour

In order to reduce the number of fitted parameters in the mathematical fitting procedure, the yield stress value was first experimentally determined from stress–strain curves. Fig. 3 shows the plastic deformation curves obtained in compression, for pastes A and B. Lubricant and plasticizer additions and extrusion water were adjusted so that the same bulk yield value ($\sigma_0 = 0.05$ MPa) was obtained.[15] The pastes exhibited different plastic behaviour, paste A being slightly less plastic than the paste B, hence requiring a slightly lower amount of extrusion water (21.5% humidity for A paste and 23.8% humidity for B paste) to reach the same σ_0 value. This difference is probably due to the use of a lower amount of W-sludge in the A formulation. It has already been shown[15] that the water content strongly affects the plastic behaviour.

The Benbow–Bridgwater's equations for the flow of pastes through dies with complex geometry[13,14,18] were used to characterise the extrusion process, as detailed in Fig. 1. Given the geometrical similarity between the two dies used in this work, the pressure difference between them, $P_{120L} - P_{30L}$, is given by Eq. (5):

$$P_{120L} - P_{30L} = (\tau_0 + \beta V^m)\frac{4(L_{120L} - L_{30L})}{d_0 - d_i} \quad (5)$$

In the present case, $L_{120L} - L_{30L} = 79.27$ mm. Eq. (5) includes only three fitting parameters, namely, τ_0, β and m, which can be iteratively calculated (least squares fitting) from extrusion data collected at different speeds. Once τ_0, β and m are known, two further parameters (α and n) can be obtained from Eqs. (3) and (4). As mentioned earlier, the yield value (σ_0) is determined from the stress–strain curves shown in Fig. 3.

Fig. 4 shows the pressure difference between the 120*L* and 30*L* dies for the two pastes A and B, both determined experimentally and calculated from Eq. (5). The departure (%) between pre-

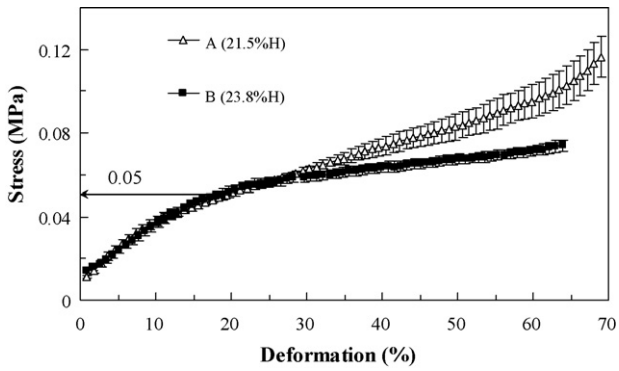

Fig. 3. Stress–strain curves of pastes A and B, obtained in compression.

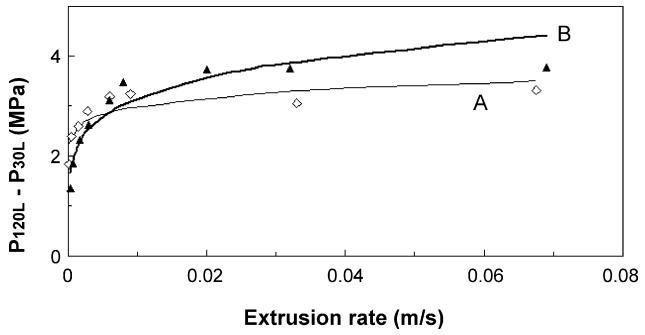

Fig. 4. Evolution of the pressure difference between 120*L* and 30*L* dies, for pastes A and B, as a function of the extrusion rate. Measured (points) and fitted (lines) results are shown.

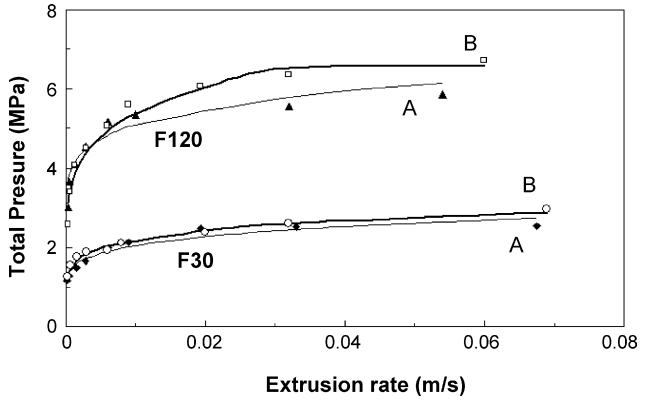

Fig. 5. Evolution of the total pressure, for pastes A and B with 120*L* and 30*L* dies, as a function of the extrusion rate. Measured (points) and fitted (lines) results are shown.

dicted (calculated) and experimental results can be accessed in terms of [100 × (predicted − experimental)/experimental]. Significant differences (23% for paste A and 24% for paste B) can be observed only at low extrusion rates (1 and 2 mm/min ram speed), most likely due to the poorer control of experimental conditions at those low rates.

Results of the full fitting procedure, obtained from Eqs. (3) and (4), are shown in Fig. 5. A general good agreement can be observed between measured values and the curves predicted by the model. The total pressure is higher for the 120*L* die due to its longer length. Despite some differences in the curve shape, the two pastes showed a similar general behaviour.

Table 2
Benbow–Bridgwater extrusion parameters for pastes A and B (σ_0 was obtained from stress–strain curves)

Parameter	A + 8% C28 + 2% O59 (21.5% H)	B + 8% C28 + 2% O59 (23.8% H)
α [MPa (s m^{-1})^n]	0.6676	0.4059
n	0.259	0.138
β [MPa (s m^{-1})^m]	0.0463	0.0838
m	0.095	0.179
τ_0 (MPa)	0.0056	0.0005
σ_0 (MPa)	0.050	0.050
μ	0.112	0.010

Table 2 shows the various parameters, experimentally determined and estimated through mathematical fitting of Eqs. (3)–(5). It is interesting to observe that the estimates obtained for pastes A and B are very similar and close to those reported by Benbow et al.[13] for α-alumina-based pastes. This suggests that both waste-based formulations are suitable for complex extrusion. Also, the water content in the final formulations is perfectly comparable to that used in the extrusion of several industrial ceramic pastes. However, the presence of 10% of organic additives might require special care during drying and firing to prevent failure at these stages.

According to Das et al.[19], n values in the range 0.2–0.6 correspond to predominantly pseudo-plastic behaviour, although values below 0.4 are recommended for the extrusion of bodies with intricate shapes such as honeycomb structures. In fact, it is desirable that the apparent viscosity stays low inside the die, to aid the paste distribution along the die body, and then increase as the extrudate emerges from the die, so that the desired shape is retained. In this study, the n estimate for paste A ($n = 0.259$) is within the desired range. The lower n value for the B paste ($n = 0.138$) suggests an easier paste flow across the internal die body and a better retention of the desired final shape.

Some authors[13,14] argue that extrusion results can be interpreted based on the α and β parameters alone, as long as they reflect dimensional effects. Alternatively, Das et al.[19] suggest the use of dynamic stress components (αV^n, describing the paste mobility during convergent flow, and βV^m, describing the paste mobility during parallel flow) while keeping the extrusion rate constant.

The general similarity between the behaviours of the two pastes is confirmed by the analysis of dynamic stress components (Fig. 6) since the convergent flow contribution is dominant in both (αV^n is higher than βV^m). However, while the βV^m component for the A paste is always lower than that for B paste, for extrusion rates higher than ~0.018 m/s the aV^n component for the A paste becomes higher than that for the B paste, which is an indication of easier flowability in the convergent geometries for composition A. This was suggested before by the stress–strain curves in Fig. 3, in which the A paste denotes lower plasticity level for similar bulk yield values (σ_0).

Table 2 also shows the estimates for the static friction coefficient (μ) of the extrudates. The A paste exhibited higher values

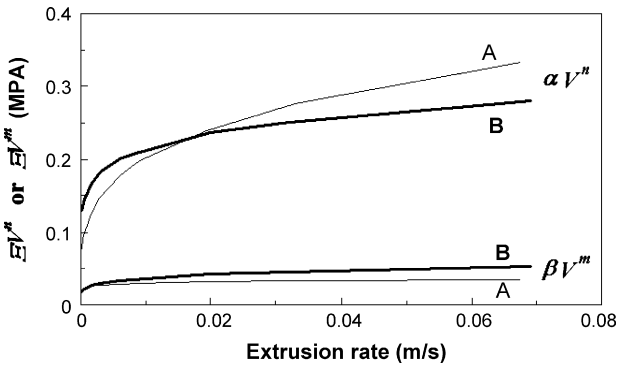

Fig. 6. Evolution of the dynamic stress components (αV^n and βV^m) for pastes A and B (30*L* die), as a function of the extrusion rate.

Table 3
Relevant physical characteristics of extruded samples of composition A, after drying and firing at the temperatures shown

Green density(g/cm^3)		2.16	
Drying shrinkage (%)		2.6	
Firing temperature (°C)	1350	1450	1550
Firing shrinkage (%)	13.5	17.4	16.9
Flexural strength (MPa)	81.7	101.8	83.7
Water absorption (%)	9.6	4.5	3.6
Apparent density (g/cm^3)	3.02	3.53	3.62

Table 4
Relevant physical characteristics of extruded samples of composition B, after drying and firing at the temperatures shown

Green density (g/cm^3)		1.97	
Drying shrinkage (%)		5.9	
Firing temperature (°C)	1350	1400	1450
Firing shrinkage (%)	1.8	10.0	16.4
Flexural strenght (MPa)	16.1	45.8	50.6
Water absorption (%)	32.9	15.8	0.61
Apparent density (g/cm^3)	1.82	2.70	*

*Samples sintered at 1450 °C show a bottom layer of adhered alumina powder, used as a refractory bed.

than the B paste (one order of magnitude), which would suggest greater resistance to the initial flow near the internal wall on die-land region for A paste. These results are related with the τ_O values, where a similar difference is observed, also suggesting the importance of this parameter. As reported in a previous work,[20] the higher μ value indicates lower surface quality for A extrudates, and can be related with the differences in the composition.

3.2. Characterisation of functional properties of the extruded bodies

Drying shrinkage of B specimens is higher than that of A specimens (5.9 and 2.6%, respectively). The higher amount of W-sludge in B paste (20%, see Table 1) might partially explain this difference, since this sludge contains fine clay particles.[9] At the same time, the water content used for the extrusion of B paste is also slightly higher and its removal during drying might induce stronger dimensional variations. Even so, when compared with common industrial ceramic pastes,[21] the shrinkage value is quite low and does not require special care during this operation.

Functional properties of sintered samples are shown in Tables 3 and 4. Interesting predictions of the effect of sintering temperature can be obtained by analysing the location of compositions in the phase diagram of the SiO_2–Al_2O_3–CaO system. Both compositions lie in the compatibility triangle C_2AS–CAS_2–CA_6 ($2CaO{\cdot}Al_2O_3{\cdot}SiO_2$–$CaO{\cdot}Al_2O_3{\cdot}2SiO_2$–$CaO{\cdot}6Al_2O_3$) shown in Fig. 7. Composition A, containing 70 wt.% A-sludge, is richer in alumina and requires higher sintering temperatures to reach significant densification levels. Its initial melting temperature is 1380 °C and it lies in primary phase field of CA_6. Mixture B, containing only 30 wt.% A-sludge and higher amounts of fluxing constituents,[21] lies on the Alkemade line between CAS_2 and C_2AS (melting begins at 1385 °C), on the CAS_2 primary phase field. In the presence of the other mixture constituents, all equilibria are expected to occur at temperatures lower than those pointed out, namely, the onset of melting is expected earlier. The role of the liquid phase present at the sintering temperature is expectably crucial to understand the differences between the two compositions.

The linear firing shrinkage of A samples (Table 3 and Fig. 8A) increases from 13.5% to a maximum of 17.4% at 1450 °C. The further increase of the sintering temperature to 1550 °C induces some expansion (decrease in the linear shrinkage), suggesting the occurrence of overfiring. This event is also inferred from the observed decrease in bending strength (from ~100 to ~80 MPa.

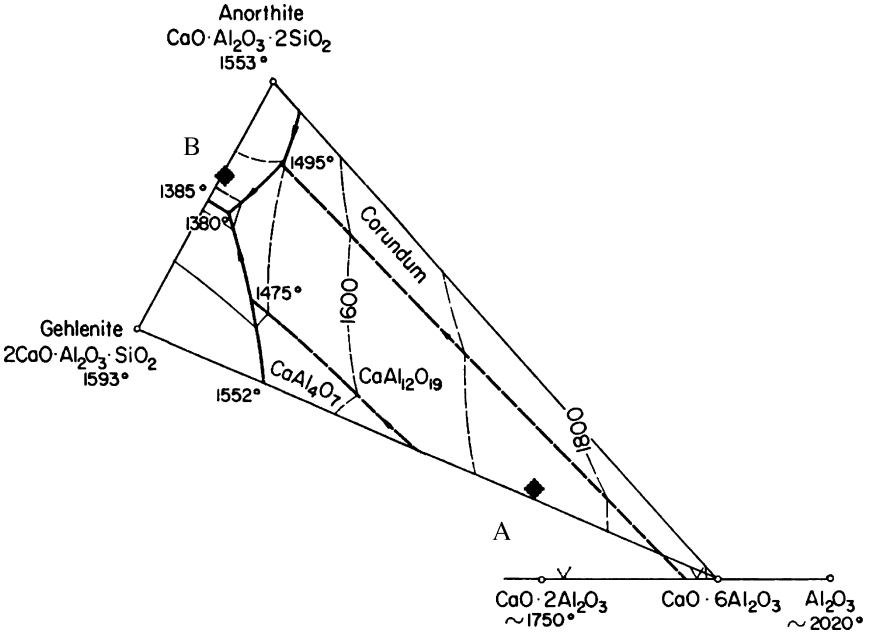

Fig. 7. Compatibility triangle C_2AS–CAS_2–CA_6 ($2CaO{\cdot}Al_2O_3{\cdot}SiO_2$–$CaO{\cdot}Al_2O_3{\cdot}2SiO_2$–$CaO{\cdot}6Al_2O_3$), showing the location of compositions A and B.

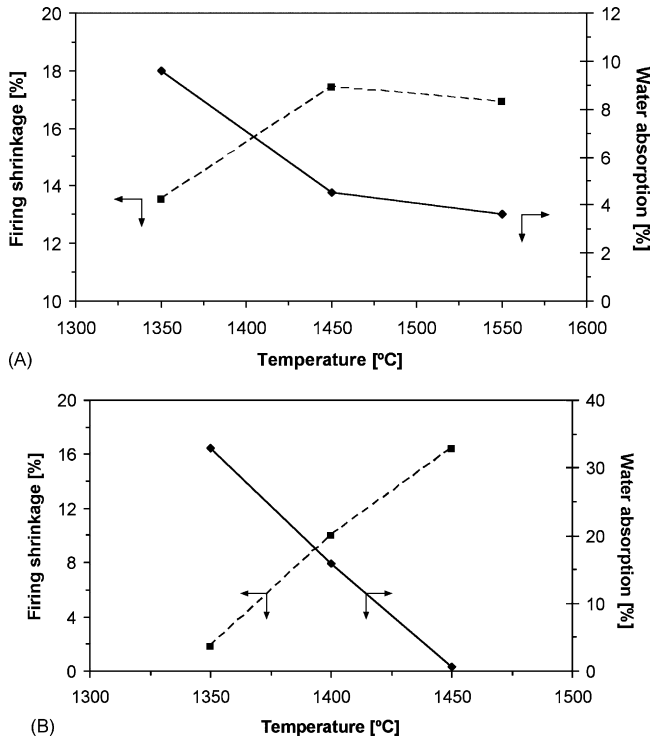

Fig. 8. Evolution of samples shrinkage and water absorption as a function of the firing temperature: (A) composition A and (B) composition B.

By recalling that melting begins at 1380 °C, the liquid formed above 1450 °C is expected to be rather abundant, explaining the overfiring signs. However, this event is not very pronounced or did not affect the samples external or surface layers, as suggested by the continuous decrease of water absorption and by the increase of the apparent density values when the firing temperature increases from 1450 to 1550 °C.

The changes with the firing temperature, in the properties of samples of the composition B are monotonous and more pronounced (Table 4). In particular, variations of the linear shrinkage and the water absorption values are very expressive (Fig. 8B) while changes in the flexural strength are much smoother above 1400 °C. Those abrupt variations indicate that this composition matures in a reasonable narrow firing interval, deserving a careful control of the experimental conditions. The differences in the maximum apparent density between composition A and composition B are those expected when considering the major phases present (respectively, CA_6, with a density of 3.84, in A, and anorthite, whose theoretical density is 2.76, in B). However, the densification level of well matured B samples (fired at 1450 °C) is higher then that of A materials (fired at 1550 °C) and the explanation for the significant differences in the maximum flexural strength of the two compositions should be searched for in microstructural details, namely, grain size and shape, in addition to compositional differences.

Figs. 9 and 10 show representative SEM views of samples A and B, respectively, sintered at different temperatures. Samples A show the presence of a lower amount of glassy phase, relative to samples B, even at the maximum sintering temperature (1550 °C) and prismatic grains are visible and are well developed. By contrast, samples B show a featureless microstructure, denoting the abundant presence of a glassy phase and dispersed small grains. Microstructure evolution (e.g., pore suppression, changes in the relative amount of glassy phase) caused by a rising

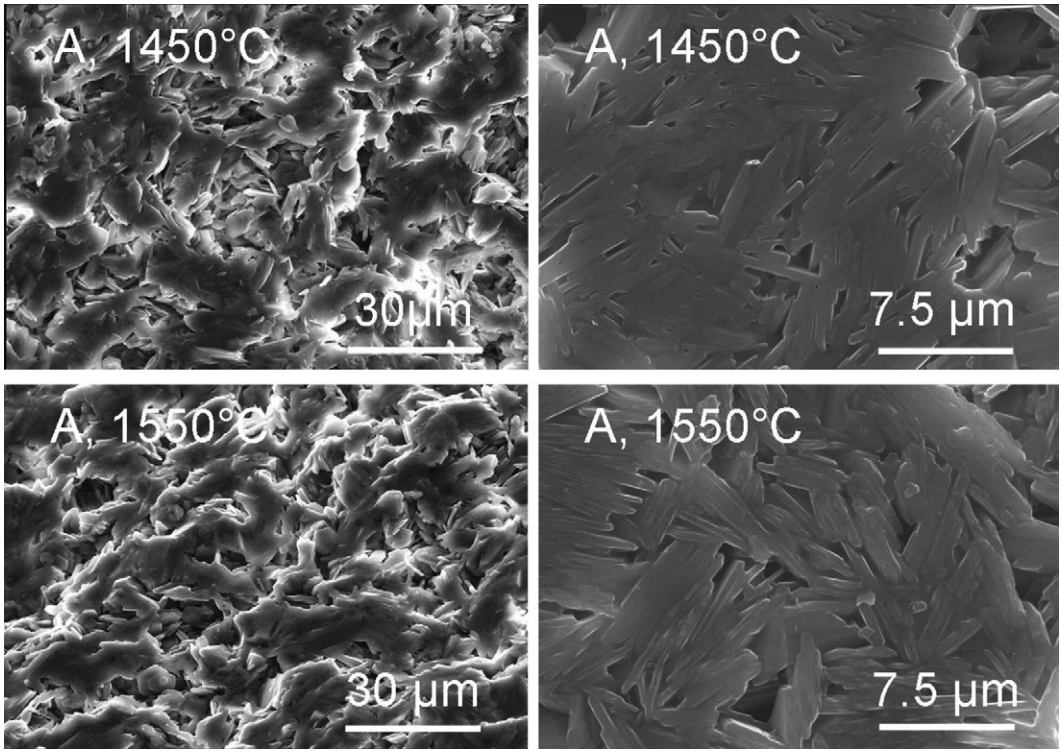

Fig. 9. Representative SEM views of samples of composition A, sintered at 1450 and 1550 °C. The micrographs on the right are polished and thermal etched surface views.

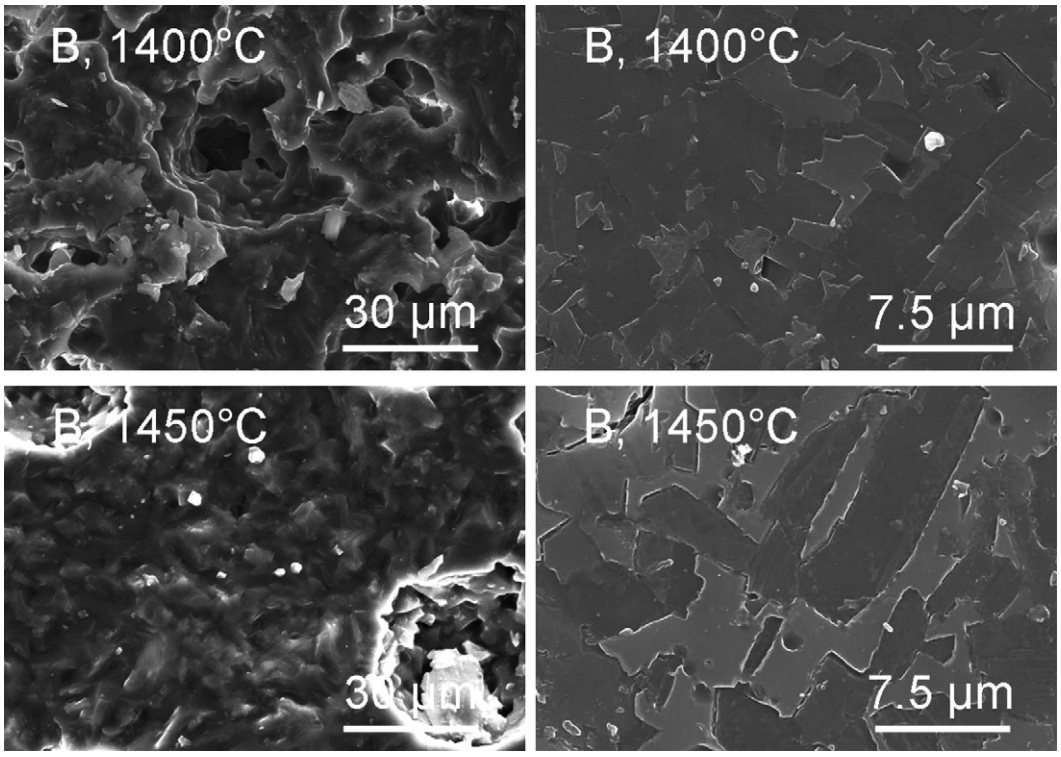

Fig. 10. Representative SEM views of samples of composition B, sintered at 1400 and 1450 °C. The micrographs on the right are polished and thermal etched surface views.

sintering temperature is much stronger in B samples, explaining the abrupt variation of physical properties (see Table 4). The theoretical cation distribution in anorthite (CAS_2) is 37 Si:27 Ca:36 Al (wt.%) and in ghelenite (C_2AS) is 17 Si:49 Ca:33 Al (wt.%). Elemental analysis carried out by EDS on B samples sintered above 1400 °C resulted in ∼9 wt.% Si, ∼18 wt.% Ca, and ∼14 wt.% Al (or 22 Si:44 Ca:34 Al) suggests that gehlenite is the major phase present.

Phase diagram analysis for composition A predicts that, after melting begins, the mixture will contain one liquid phase in equilibrium with two solids: CA_6 (hibonite, $CaO{\cdot}6Al_2O_3$) + C_2AS (gehlenite, $2CaO{\cdot}Al_2O_3{\cdot}SiO_2$) up to 1475 °C. Between 1475 and ∼1600 °C, the material should contain a liquid phase in equilibrium with $CA_6 + CA_2$. The micrographs in Fig. 9 clearly show the typical morphology of hibonite (CA_6) crystals. Fig. 11 shows phase changes in composition A as a function of the sintering temperature. At 1350 °C, the material still contains residual alumina, together with gehlenite and hibonite. With the rise in temperature (1450 °C), residual alumina content decreases and CA_6 content increases at the expenses of that of C_2AS. The presence of anorthite (CAS_2, $CaO{\cdot}Al_2O_3{\cdot}2SiO_2$) is also detected. At 1550 °C the main crystalline phase detected is CA_6 but anorthite is still present and CA_2 was not detected. This analysis suggests that full equilibrium has not been reached in this mixture.

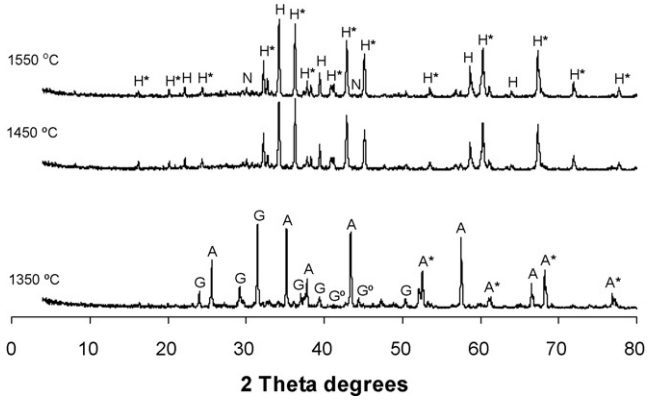

Fig. 11. Evolution of phases in composition A as a function of the firing temperature: A, alumina; A*, A + G; G, gehlenite; G°, G + H; H, hibonite; H*, H + N and N, anorthite.

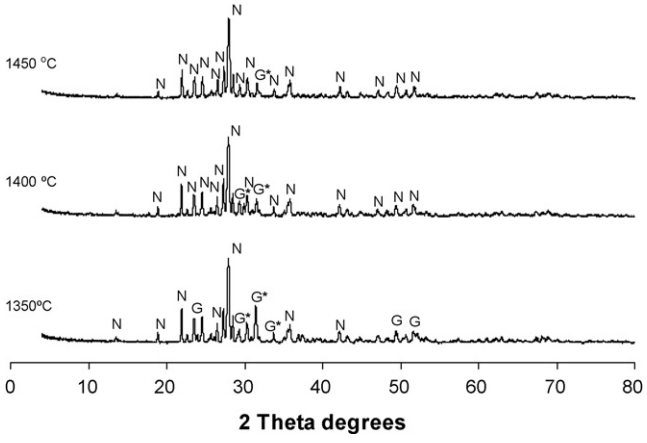

Fig. 12. Evolution of phases in composition B as a function of the firing temperature: G (gehlenite), G* (G + N) and N (anorthite).

The general similarity of X-ray patterns of samples sintered at 1450 and 1550 °C agrees in some extent with the slow change of the physical/functional properties in that temperature range.

Fig. 12 shows phase changes in mixture B as a function of the sintering temperature. As suggested by the phase diagram (Fig. 7), both CAS_2 and C_2AS were detected in the X-ray diffractogram at 1350 °C but with increasing temperature the amount of anorthite tend to increase over that of gehlenite, which the EDS analysis suggested was the major phase present. At 1450 °C, only traces of gehlenite seem to be present. The change from 1400 to 1450 °C is still important which agrees with the observed changes on functional properties.

4. Conclusions

The combination of several industrial wastes and conventional shaping techniques, such as extrusion, is a promising way to produce sintered ceramic materials with potential interest for uses like refractories (based on CA_6) or electrical insulators. The design of interesting technological properties (e.g. high electrical resistance, mechanical strength, refractoriness) was found to be easily achievable by controlling the initial batch formulation and/or the sintering schedule.

After careful study, the adaptability of two different formulations for extrusion shaping was demonstrated. Additives such as plasticizers and lubricants were added to enhance the plasticity and improve the extrudability of both pastes. The required amount of water was close to common values for industrial-type pastes. The experimental measurements of extrusion-dependent variables of both pastes are in good agreement with values predicted by Benbow–Bridgwater's model. The Benbow–Bridgwater's fitting parameters (α, β, m, n and τ_0) give a valuable indication about the dominant flow type in different die regions. The static friction coefficient, μ, was found to be the most sensitive parameter to distinguish the extrusion behaviour between the two optimised formulations. Values were found to be in the recommended range for extrusion of complex shapes.

Acknowledgements

This work was supported by FCT (Project CTA/42448/2001) and CAPES–MEC, Brazil (F. Raupp-Pereira, Ph.D. grant).

References

1. Ribeiro, M. J., Tulyaganov, D. U., Ferreira, J. M. and Labrincha, J. A., Recycling of Al rich industrial sludge in refractory ceramic pressed bodies. *Ceram. Int.*, 2002, **28**(3), 319–326.
2. Martelon, E., Jarrige, J., Ribeiro, M. J., Ferreira, J. M. and Labrincha, J. A., New clay-based ceramic formulations containing different solid wastes. *Ind. Ceram.*, 2000, **20**(2), 71–76.
3. Tulyaganov, D. U., Olhero, S. M. H., Ribeiro, M. J., Ferreira, J. M. F. and Labrincha, J. A., Mullite-alumina refractory ceramics obtained from mixtures of natural common materials and recycled Al-rich anodizing sludge. *J. Mat. Synt. Proc.*, 2002, **10**, 311–318.
4. Pereira, D. A., Couto, D. M. and Labrincha, J. A., Incorporation of aluminum-rich residues in refractory bricks. *Ceram. Forum Int.*, 2000, **77**, 21–25.
5. Magalhães, J. M., Silva, J. E., Castro, F. P. and Labrincha, J. A., Kinetic study of the immobilization of galvanic sludge in clay-based matrix. *J. Hazard. Mater.*, 2005, **121**(1–3), 69–78.
6. Perez, J. A., Terradas, R., Manent, M. R., Seijas, M. and Martinez, S., Inertization of industrial wastes in ceramic materials. *Ind. Ceram.*, 1996, **16**, 7–10.
7. Dondi, M., Marsigli, M. and Fabbri, B., Recycling of industrial and urban wastes in brick production—a review. *Tile Brick Int.*, 1997, **13**, 302–308.
8. Raupp-Pereira, F., Nunes, A. F., Segadães, A. M. and Labrincha, J. A., Refractory mortars made of different wastes and natural sub-products. *Key Eng. Mater.*, 2004, **264–268**, 1743–1746.
9. Raupp-Pereira, F., Hotza, D., Segadães, A. M. and Labrincha, J. A., Recycling of several wastes as refractory materials. In *Proceedings of UNITECR'03*, ed. TARJ, 2003, pp. 150–153.
10. Nunes, P., Ribeiro, M. J., Ferreira, J. M. F., Bóia, C. S. and Labrincha, J. A., Mullite-based materials obtained from industrial wastes and natural sub-products. In *Proceedings of TMS Fall Meeting on Recycling and Waste Treatment in Mineral and Metal Processing: Technical and Economic Aspects, vol. 2*, ed. B. Bjorkman, C. Samuelsson and J. Wikstrom, 2002, pp. 359–368.
11. Ferreira, J. M. F., Torres, P. M. C., Silva, M. S. and Labrincha, J. A., Recycling of sludges generated from natural stones cutting processes in ceramic formulations. In *Proceedings of TMS Fall Meeting on Recycling and Waste Treatment in Mineral and Metal Processing: Technical and Economic Aspects, vol. 2*, ed. B. Bjorkman, C. Samuelsson and J. Wikstrom, 2002, pp. 389–395.
12. Raupp-Pereira, F., Hotza, D., Segadães, A. M. and Labrincha, J. A., Ceramic formulations made of different wastes and natural sub-products. *Ceram. Int.*, 2006, **32**, 173–179.
13. Benbow, J. J., Oxley, E. W. and Bridgwater, J., The extrusion mechanics of pastes—the influence of pastes formulation on extrusion parameters. *Chem. Eng. Sci.*, 1987, **42**(9), 2151–2162.
14. Benbow, J. J., Lawson, T. A., Oxley, E. W. and Bridgwater, J., Prediction of paste extrusion pressure. *Ceram. Bull.*, 1989, **68**(10), 1821–1824.
15. Ribeiro, M. J., Ferreira, J. M. and Labrincha, J. A., Plastic behaviour of different ceramics pastes processed by extrusion. *Ceram. Int.*, 2005, **31**, 515–519.
16. Ribeiro, M. J., Albuquerque, C. M., Ferreira, J. M. F., Labrincha, J. A. and Labrincha, J. A., Cordierite-based extruded bodies made from aluminium-rich anodising sludge and natural sub-products. In *Proceedings of REWAS'04, Global Symposium on Recycling, Waste Treatment and Clean Technology, vol. 1*, ed. I. Gaballah, B. Mishra, R. Solozabal and M. Tanaka, 2004, pp. 215–224.
17. Wight Jr., J. F. and Reed, J. S., Nonaqueous aluminium nitride extrusion: II, die-land flow and tribology. *J. Am. Ceram. Soc.*, 2002, **85**, 1689–1694.
18. Benbow, J. J., Jazayeri, S. H. and Bridgwater, J., The flow of pastes through dies of complicated geometry. *Powder Technol.*, 1991, **65**, 393–401.
19. Das, R. N., Madhusoodana, C. D. and Okada, K., Rheological studies on cordierite honeycomb extrusion. *J. Eur. Ceram. Soc.*, 2002, **22**, 2893–2900.
20. Ribeiro, M. J., Blackburn, S., Ferreira, J. M. and Labrincha, J. A., Extrusion of alumina and cordierite-based tubes made from Al-rich anodizing sludge. *J. Eur. Ceram. Soc.*, 2006, **26**, 817–823.
21. Barsoum, M., *Fundamentals of Ceramics*. McGraw-Hill International Editions, Singapore, 1997, pp. 331–390.